12

NEUTRON PHYSICS

As the uncharged member of the nucleon pair, the neutron plays a fundamental role in the study of nuclear forces. Unaffected by the Coulomb barrier, neutrons of even very low energy (eV or less) can penetrate the nucleus and initiate nuclear reactions. In contrast, part of our lack of understanding of processes in the interior of stars results from the difficulty of studying proton-induced reactions at energies as low as keV. On the other hand, the lack of Coulomb interaction presents some experimental problems when using neutrons as a nuclear probe: energy selection and focusing of an incident neutron beam are difficult, and neutrons do not produce primary ionization events in detectors (neutrons passing through matter have negligible interactions with the atomic electrons).

The first experimental observation of the neutron occurred in 1930, when Bothe and Becker bombarded beryllium with α particles (from radioactive decay) and obtained a very penetrating but nonionizing radiation, which they assumed to be a high-energy γ ray. Soon thereafter, Curie and Joliot noticed that when this radiation fell on paraffin, an energetic proton was emitted. From the range of these protons, they determined their energy to be 5.3 MeV. If the radiation under study were indeed γ's, protons could be knocked loose from paraffin by a Compton-like collision; from the Compton-scattering formula, they computed that the energy of this "γ radiation" would be at least 52 MeV to release such protons. An emitted γ of such an energy seemed extremely unlikely. In 1932, Chadwick provided the correct explanation, identifying the unknown radiation as a neutral (therefore penetrating and nonionizing) particle with a mass nearly the same as that of the proton. Thus in a head-on collision, a 5.3-MeV neutron could transfer its energy entirely to the struck proton. Chadwick did additional recoil experiments with neutrons and confirmed his hypothesis, and he is generally credited with being the discoverer of the neutron.

The free neutron is unstable against β decay, with a half-life of 10.6 min. In nuclei, the bound neutron may be much longer-lived (even stable) or much shorter-lived. Despite the instability of free neutrons, their properties are measured to high precision, particularly the magnetic dipole moment, $\mu = -1.91304184 \pm 0.00000088\ \mu_N$, and the neutron-proton mass difference, $m_n - m_p = 1.29340 \pm 0.00003$ MeV.

Basic research with neutrons goes back almost to the earliest days of nuclear physics, and it continues to be a vital and exciting research field today. For example, interference effects with neutron beams have permitted some basic

aspects of quantum mechanics to be demonstrated for the first time. The *electric* dipole moment of the neutron should vanish if the neutron were an elementary particle or even a composite particle in which the binding forces were symmetric with respect to the parity and time-reversal operations. Many careful and detailed experiments have been done, and all indicate a vanishing electric dipole moment, but the limit has been pushed so low (10^{-25} e · cm) that it is almost possible to distinguish among certain competing theories for the interactions among the elementary particles. The so-called Grand Unified Theories that attempt to unify the strong (nuclear), electromagnetic, and weak (β-decay) interactions predict that the conservation of nucleon number (actually baryon number) can break down, and that a neutron could convert into its antiparticle, the antineutron, and then back again to a neutron. No evidence has yet been seen for this effect either, but current research is trying to improve the limits on our knowledge of the neutron-antineutron conversion frequency.

12.1 NEUTRON SOURCES

Beams of neutrons can be produced from a variety of nuclear reactions. We cannot accelerate neutrons as we can charged particles, but we can start with high-energy neutrons and reduce their energy through collisions with atoms of various materials. This process of slowing is called "moderating" the neutrons. The resulting neutrons can have very low energies, which by convention are given the following designations:

Thermal	$E \simeq 0.025$ eV
Epithermal	$E \sim 1$ eV
Slow	$E \sim 1$ keV
Fast	$E = 100$ keV–10 MeV

α-Beryllium Sources The reaction responsible for the discovery of the neutron can be used to produce a source of neutrons suitable for use in the laboratory. The stable isotope of beryllium, ^{9}Be, has a relatively loosely bound neutron (1.7 MeV binding energy). If a typical α particle from a radioactive decay (5–6 MeV) strikes a ^{9}Be nucleus, a neutron can be released:

$$^4\text{He} + {}^9\text{Be} \rightarrow {}^{12}\text{C} + \text{n}$$

The Q value for this reaction is 5.7 MeV. If we mix together a long-lived α-emitting material, such as ^{226}Ra, and ^{9}Be, there will be a constant rate of neutron production. From ^{226}Ra and its daughters there are α's emitted with energies from about 5 to nearly 8 MeV, and thus we find neutrons with an energy spectrum up to 13 MeV. The neutrons are not monoenergetic because of (1) the many α groups, (2) the slowing of α's that will occur by collision in any solid material, (3) the various directions of emission that can occur for the neutrons relative to the α's (whose direction we do not know), and (4) the possibility that ^{12}C is left in an excited state. The most probable neutron energy is about 5 MeV, and the neutron production rate is about 10^7 neutrons per second for each Ci of ^{226}Ra. A typical neutron spectrum is shown in Figure 12.1.

Because of the high γ emission of ^{226}Ra and its daughters, the radium-beryllium neutron source has largely been replaced with sources using ^{210}Po (138 d),

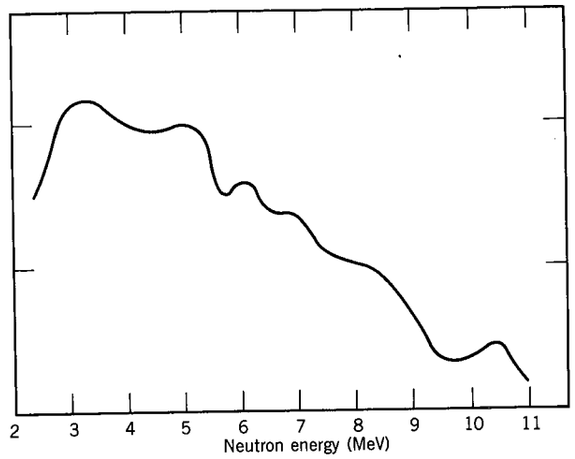

Figure 12.1 Neutron energy spectrum from a Ra-Be source, measured with a proton recoil counter. Several neutron groups are present; they result from reactions induced by α's with differing energies and in which the ^{12}C is left either in the ground state or the 4.43- or 7.6-MeV excited states.

^{238}Pu (86 y), and ^{241}Am (458 y). These sources produce about $2–3 \times 10^6$ neutrons per second per Ci of α activity.

Photoneutron Sources In a process similar to the (α, n) sources discussed above, we can use the (γ, n) reaction to produce neutrons. The advantage of photoneutron production is that we can make the neutrons more nearly monoenergetic, particularly if the photon source is nearly monoenergetic. For example, ^{24}Na emits a γ of 2.76 MeV, absorption of which would be sufficient to overcome the neutron binding energy of ^9Be:

$$\gamma + {}^9\text{Be} \rightarrow {}^8\text{Be} + \text{n}$$

The yield is acceptable (2×10^6 neutrons/s per Ci of ^{24}Na), but the half-life is short (15 h). The neutron energy is about 0.8 MeV. A longer-lived isotope ^{124}Sb (60 d) emits a strong γ whose energy just exceeds the ^9Be neutron binding energy; the emitted neutron has a much lower energy, about 24 keV.

Spontaneous Fission A common source of neutrons is the spontaneous fission of isotopes such as ^{252}Cf (2.65 y). Neutrons are produced directly in the fission process, at a rate of about 4 per fission. The fission occurs in only about 3% of the decays (α decay accounts for the rest), and the neutron production rate is 2.3×10^{12} neutrons/s per gram of ^{252}Cf or 4.3×10^9 n/s per Ci of ^{252}Cf. The neutron energies are characteristic of fission—a continuous distribution with an average energy of 1–3 MeV.

Nuclear Reactions There are of course many nuclear reactions that produce neutrons. These require an accelerator to produce a beam of particles to initiate the reaction, and thus they are not as convenient as the radioactive-decay type of sources discussed previously. However, by carefully selecting the incident energy and the angle at which we observe the emitted neutron, we can obtain a

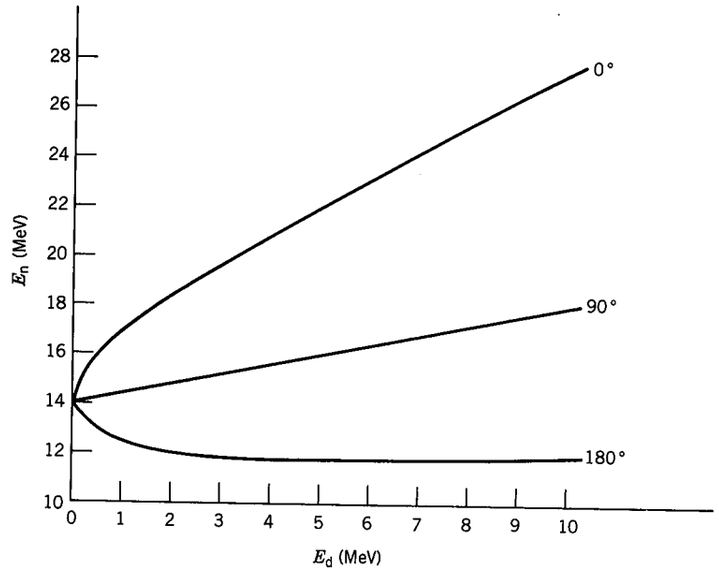

Figure 12.2 Neutrons emitted in the $^3H(d, n)^4He$ reaction.

reasonably monoenergetic beam of almost any desired energy. Some reactions that might be used are

$$^3\text{H} + \text{d} \rightarrow {}^4\text{He} + \text{n} \qquad Q = +17.6 \text{ MeV}$$
$$^9\text{Be} + {}^4\text{He} \rightarrow {}^{12}\text{C} + \text{n} \qquad Q = +5.7 \text{ MeV}$$
$$^7\text{Li} + \text{p} \rightarrow {}^7\text{Be} + \text{n} \qquad Q = -1.6 \text{ MeV}$$
$$^2\text{H} + \text{d} \rightarrow {}^3\text{He} + \text{n} \qquad Q = +3.3 \text{ MeV}$$

Figure 12.2 illustrates the dependence of the neutron energy in the first of these reactions on the incident energy and on the direction of the outgoing neutron.

Reactor Sources The neutron flux near the core of a nuclear fission reactor can be quite high—typically 10^{14} neutrons/cm^2/s. The energy spectrum extends to 5–7 MeV but peaks at 1–2 MeV. These neutrons are generally reduced to thermal energies within the reactor, but there are also fast neutrons present in the core. Cutting a small hole in the shielding of the reactor vessel permits a beam of neutrons to be extracted into the laboratory for experiments. The high neutron fluxes from a reactor are particularly useful for production of radioisotopes by neutron capture, as in neutron activation analysis.

12.2 ABSORPTION AND MODERATION OF NEUTRONS

As a beam of neutrons travels through bulk matter, the intensity will decrease as neutrons are removed from the beam by nuclear reactions. For fast neutrons, many reactions such as (n, p), (n, α), or (n, 2n) are possible, but for slow or thermal neutrons the primary cause of their disappearance is capture, in the form

of the (n, γ) reaction. Often the cross sections for these capture reactions are dominated by one or more resonances, where the cross section becomes very large. Off resonance, the cross section decreases with increasing velocity like v^{-1}; thus as the neutrons slow down (become moderated) due to elastic and inelastic scattering processes, absorption becomes more probable. Neutrons with initial energy in the 1-MeV range would undergo many scattering processes until their energies were reduced to the eV range, where they would have a high probability of resonant or nonresonant absorption.

In crossing a thickness dx of material, the neutrons will encounter $n\,dx$ atoms per unit surface area of the beam or the material, where n is the number of atoms per unit volume of the material. If σ_t is the total cross section (including scattering processes, which will tend to divert neutrons from the beam), then the loss in intensity I is

$$dI = -I\sigma_t n\,dx \tag{12.1}$$

and the intensity decreases with absorber thickness according to an exponential relationship:

$$I = I_0 e^{-\sigma_t n x} \tag{12.2}$$

Keep in mind that this expression refers only to monoenergetic neutrons—the original intensity of neutrons of a certain energy decreases according to Equation 12.2. Of course, we may at the same time be creating neutrons of lower energy (by scattering, for example), which may have a very different cross section, but this effect is not included in Equation 12.2. We therefore cannot use it reliably to calculate the decrease in the *total number* of neutrons, only the change in intensity of those with a given initial energy.

Let's consider an elastic collision between a neutron of initial energy E and velocity v with a target atom of mass A initially at rest. Elementary application of the laws of conservation of energy and linear momentum gives the ratio between the final neutron energy E' and the initial energy:

$$\frac{E'}{E} = \frac{A^2 + 1 + 2A\cos\theta}{(A+1)^2} \tag{12.3}$$

where θ is the scattering angle in the center-of-mass system (but E and E' are measured in the laboratory system). For no scattering ($\theta = 0$), Equation 12.3 gives $E'/E = 1$, as it should. The maximum energy loss occurs for a head-on collision ($\theta = 180°$):

$$\left(\frac{E'}{E}\right)_{\min} = \left(\frac{A-1}{A+1}\right)^2 \tag{12.4}$$

Notice that for $A = 1$ (scattering from hydrogen), the neutron gives all its energy to the struck proton.

For neutron energies of about 10 MeV and below, the scattering is mostly s wave and thus (in the center-of-mass system) largely independent of θ. The values of E'/E are uniformly distributed between $E'/E = 1$ and the minimum value given by Equation 12.4, as shown in Figure 12.3*a*.

Because each neutron will scatter many times, we must repeatedly calculate the energy loss. In the case of the second scattering, the incident neutrons are no

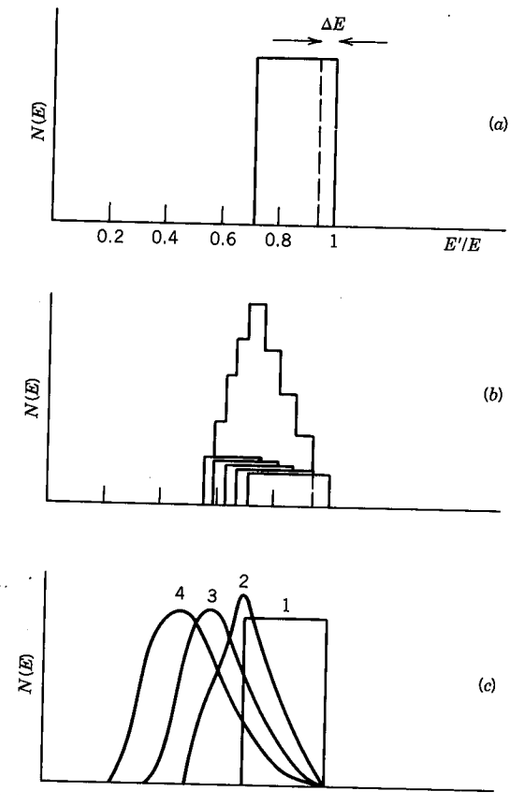

Figure 12.3 (*a*) A monoenergetic neutron of energy E gives, after a single s-wave scattering from ^{12}C, a flat distribution of laboratory energies E' from $0.72E$ to E. (*b*) Dividing the scattered distribution into five narrow, nearly monoenergetic distributions of width ΔE, we get after a second scattering the five flat distributions shown, whose sum is the peaked distribution. (*c*) An exact calculation of the energy distribution after 1, 2, 3, and 4 scatterings.

longer monoenergetic but rather are distributed as in Figure 12.3*a*. We can approximate this effect by considering each interval of width ΔE to be a new generation of approximately monoenergetic neutrons giving the result shown in Figure 12.3*b*. Continuing this process, we obtain the succeeding "generations" of energy distributions shown in Figure 12.3*c*.

To make the calculations more quantitative, we define the parameter ξ to represent the average value of $\log(E/E')$ after a single collision:

$$\xi = \left[\log\frac{E}{E'}\right]_{\text{av}} \tag{12.5}$$

$$= \frac{\int \log\left[\dfrac{(A+1)^2}{A^2 + 1 + 2A\cos\theta}\right] d\Omega}{\int d\Omega} \tag{12.6}$$

Table 12.1 Moderating Properties of Various Nuclei

Nucleus	ξ	n (for thermalization)
^{1}H	1.00	18
^{2}H	0.725	25
^{4}He	0.425	43
^{12}C	0.158	110
^{238}U	0.0084	2200

where $d\Omega$ is the element of solid angle in the center-of-mass system. Here again we assume the scattering to be isotropic. Carrying out the integration gives

$$\xi = 1 + \frac{(A-1)^2}{2A} \log \frac{A-1}{A+1} \tag{12.7}$$

The average value of $\log E'$ is decreased after each collision by an amount ξ, and after n collisions, the average value of $\log E'$ is $\log E'_n$:

$$\log E'_n = \log E - n\xi \tag{12.8}$$

which follows directly from Equation 12.5.

Table 12.1 shows values of ξ for some commonly used moderators. If our goal is to reduce the average neutron energy from that which is typical for neutrons emitted in fission ($E \sim 2$ MeV) to that which is characteristic of thermal motion ($E'_n \sim 0.025$ eV), the number of generations of collisions is shown in Table 12.1.

The previous calculation has assumed the atoms from which the neutrons scatter to be at rest. This is certainly a good approximation for MeV neutrons, but as thermal energies are approached, we find the thermal motion of the atoms of the moderator to be comparable to the speeds of the neutrons. The scattering in this case is better analyzed using statistical mechanics, and we can simply assume that after a sufficient time the neutrons will reach thermal equilibrium with the moderator at a temperature T. In this case, the neutrons are described by a Maxwellian speed distribution:

$$f(v)\,dv = 4\pi n \left(\frac{m}{2\pi kT}\right)^{3/2} v^2 e^{-mv^2/2kT}\,dv \tag{12.9}$$

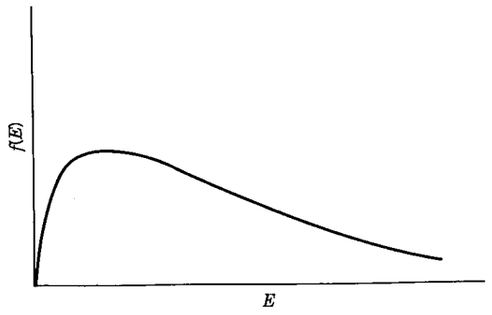

Figure 12.4 Maxwellian energy distribution, a representation of the neutron energy spectrum after many scatterings.

where $f(v)\,dv$ gives the fraction of neutrons with speeds between v and $v + dv$. Here m is the neutron mass and n is the total number of neutrons per unit volume. Rewriting this in terms of energy gives

$$f(E)\,dE = \frac{2\pi n}{(\pi kT)^{3/2}} E^{1/2} e^{-E/kT}\,dE \tag{12.10}$$

which is illustrated in Figure 12.4 and looks similar to Figure 12.3*c*, showing the thermalizing effect of even a few generations of collisions.

12.3 NEUTRON DETECTORS

Because neutrons produce no direct ionization events, neutron detectors must be based on detecting the secondary events produced by nuclear reactions, such as (n, p), (n, α), (n, γ), or (n, fission), or by nuclear scattering from light charged particles, which are then detected.

For slow and thermal neutrons, detectors based on the (n, p) and (n, α) reactions provide a direct means for observing neutrons from the signal left by the energetic p or α resulting from the reaction. The isotope ^{10}B is commonly used, by producing an ionization chamber or a proportional counter filled with BF_3 gas or lined with boron metal or a boron compound. The reaction is

$$^{10}\mathrm{B} + \mathrm{n} \rightarrow {}^{7}\mathrm{Li}^* + \alpha$$

where the ^{7}Li is preferentially left in an excited state with energy 0.48 MeV. (Natural boron consists of about 20% of the isotope ^{10}B, so materials enriched in ^{10}B increase the efficiency of the detector.) For thermal neutrons, the cross section is about 3840 b, a very large value, and the cross section follows the $1/v$ law up to about 100 keV, so the dependence of cross section on incident energy is featureless (no resonances are present) and predictable (Figure 12.5).

There is also another advantage of the $1/v$ dependence of the cross section. Suppose we are observing a collimated beam of neutrons or an isotropic flux (perhaps near the core of a reactor) that has a velocity distribution of $n(v)\,dv$ neutrons per unit volume with speeds between v and $v + dv$. The flux passing through the detector will be $n(v)v\,dv$, and if the counter contains N boron nuclei each with cross section σ, the probability per second of an interaction (or counting rate, if we are able to detect and count every interaction) is

$$dR = N\sigma n(v) v\,dv \tag{12.11}$$

for neutrons of speeds between v and $v + dv$. For neutrons of all speeds, the total counting rate is

$$R = \int N\sigma n(v) v\,dv \tag{12.12}$$

$$= NC \int n(v)\,dv \tag{12.13}$$

where the last step assumes that $\sigma \propto v^{-1}$, so that the product σv is the constant C. The integral then gives the total number of neutrons per unit volume n, and

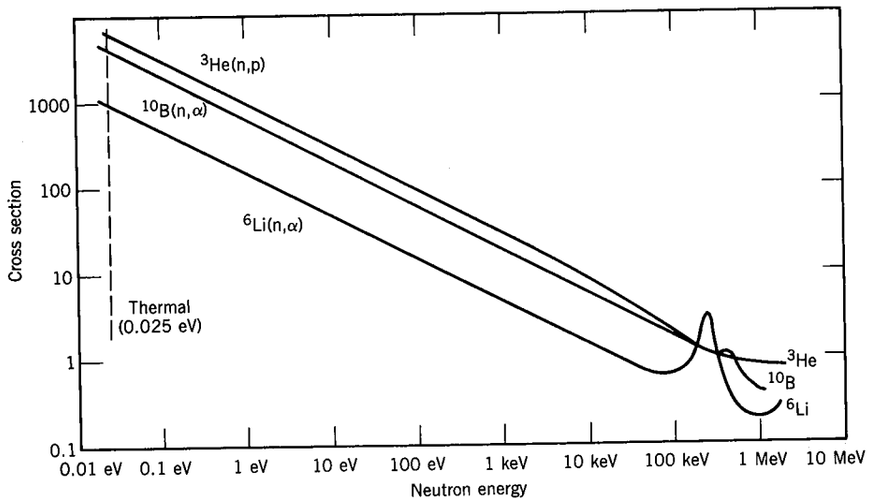

Figure 12.5 Neutron cross sections for ^{3}He(n, p), ^{10}B(n, α), and ^{6}Li(n,α). The cross section shows the $1/v$ behavior for $E < 1$ keV, but begins to show resonances above 100 keV.

the counting rate is

$$R = NCn \tag{12.14}$$

That is, R is directly proportional to the neutron density for *any distribution of velocities* as long as we can neglect any contributions to the neutron flux outside the $1/v$ region of cross section.

The Q value for the reaction leading to the ^{7}Li excited state is 2.31 MeV, and for incident neutrons of kinetic energy small compared with this value, momentum conservation requires the sharing of energy between ^{7}Li and α so that the α is given a kinetic energy of 1.47 MeV. The kinetic energy of the incident neutron, if it is in the eV or even keV range, will not substantially modify this value. Unless either particle strikes the wall, we will detect simultaneously the ^{7}Li ($T = 0.84$ MeV) as well, and the neutron then leaves as its signature a 2.31-MeV energy loss in the counter. Because we cannot measure MeV energies to eV or keV precision in a proportional counter, we cannot use such a device to measure such low neutron energies.

Other similar devices are based on ^{6}Li (n, α), with $Q = 4.78$ MeV and $\sigma = 940$ b for thermal neutrons, and ^{3}He (n, p), with $Q = 0.765$ MeV and $\sigma = 5330$ b. A comparison of the neutron cross sections for these reactions is shown in Figure 12.5.

Another way of measuring neutron intensities is by exposing to the neutrons a material which becomes radioactive after neutron capture and which has a known capture cross section for neutrons of a particular energy. If we remove the material from the neutron flux and measure the induced radioactivity (using a γ-ray detector, for example), we can determine the neutron flux.

Among the earliest devices used for determining neutron energies were mechanical devices, for example the velocity selector, a rotating shutter made of a highly absorbing material, such as Cd for thermal neutrons (Figure 12.6). This

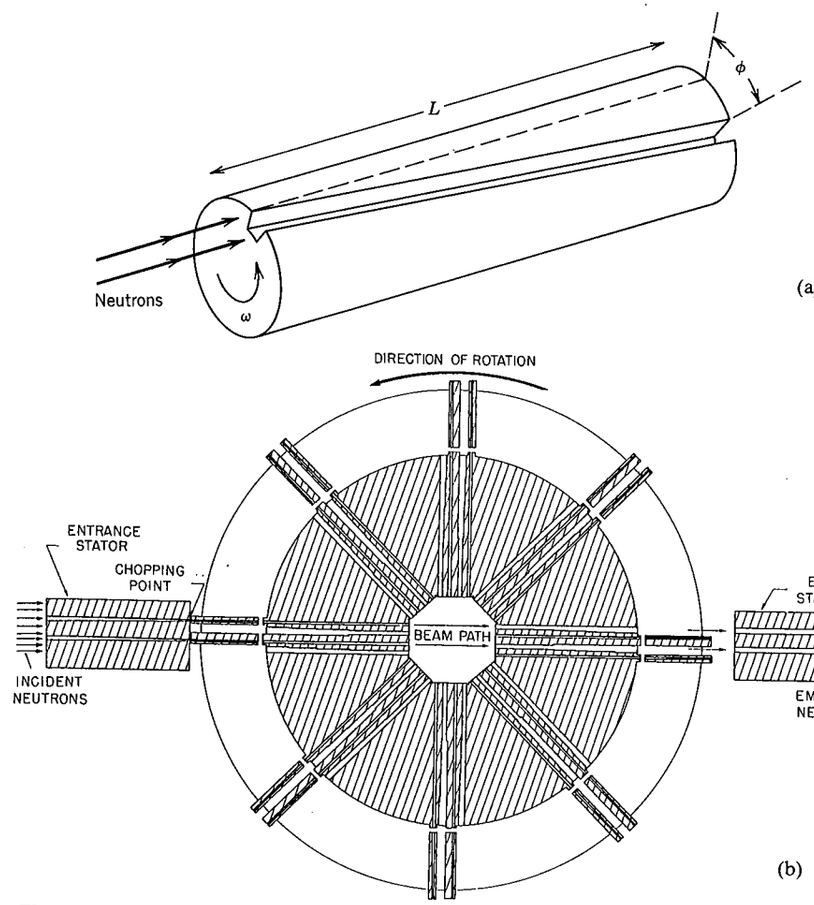

Figure 12.6 (*a*) Neutron velocity selector, consisting of a rotating cylinder with one or more helical slots cut into its surface. The cylinder is made of a material, such as cadmium, with a high absorption for neutrons. The selector will pass neutrons of velocity v that travel the length L of the cylinder in the time that it takes it to rotate through the angle ϕ; that is, $t = L/v = \phi/\omega$, so that $v = L\omega/\phi$. Changing the angular speed ω permits selection of the neutron velocity. (*b*) Rotating shutter or "chopper" for producing pulses of neutrons. A continuous stream of neutrons enters from the left and a pulse of neutrons emerges at right if the rotor slits line up with the entrance slits. The rotor is made of stainless steel with phenolic slits. From R. E. Chrien, in *Neutron Sources for Basic Physics and Applications*, edited by S. Cierjacks (Oxford: Pergamon, 1983).

device is practical only for velocities in the thermal region, but it can be used to select neutrons from the continuous velocity distribution such as is produced by a reactor.

Another way of measuring velocities is through a variant of the time-of-flight technique (see Section 7.9 and Figure 7.39). If we have neutrons in a short pulse, we can time their travel over a distance of several meters (thermal neutrons have

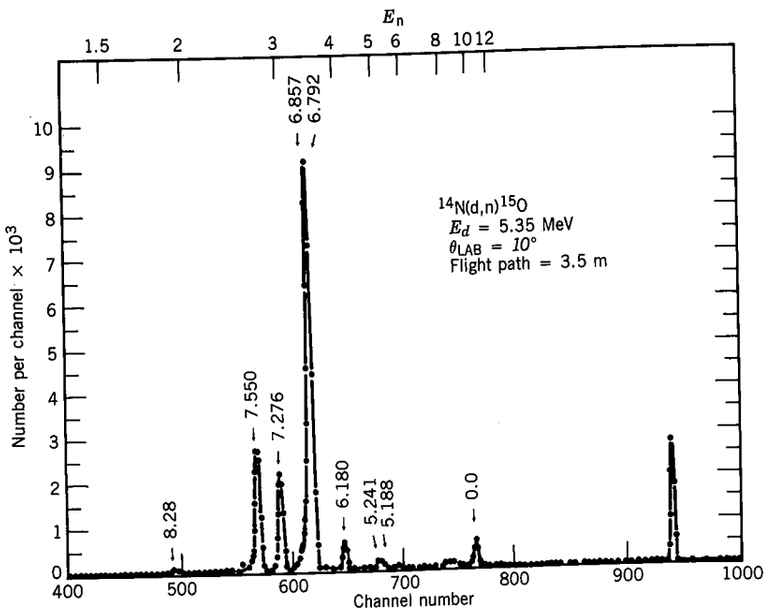

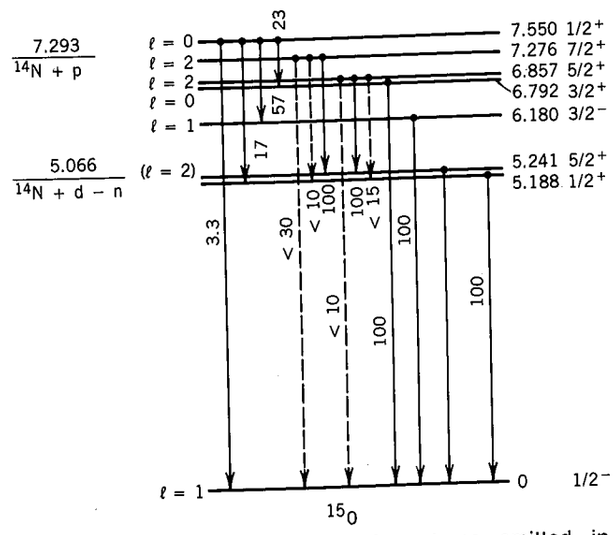

Figure 12.7 Time-of-flight spectrum of neutrons emitted in the reaction $^{14}N(d, n)^{15}O$. Timing was done with reference to a pulsed beam of deuterons. The peak at far right comes from γ rays, which of course travel at the highest possible speed. The neutron peaks correspond to the ground and excited states of ^{15}O, as shown. The ℓ values come from measurement of the angular distribution of the cross section, or $d\sigma/d\Omega$. From R. C. Ritter, E. Sheldon, and M. Strang, *Nucl. Phys.* *A* **140**, 609 (1970).

$v = 2200$ m/s, and the time of travel is thus an easily measurable 10^{-3} s). For higher energies, longer flight paths of order 100 m and increased sensitivity of short-timing techniques can give accurate velocity measurements for neutrons up to MeV energies.

The initial pulse of neutrons for a timing measurement can be provided by a "chopper" of the kind shown in Figure 12.6, or else by a pulsed charged-particle accelerator, in which the neutrons are produced through reactions such as those listed in Section 12.1. If the initial pulse includes a wide range of velocities, the start-stop technique using a time-to-amplitude converter can display the energy spectrum of the neutrons, as in Figure 12.7.

Very precise energy determinations can be done in the thermal region using crystal diffraction. Thermal neutrons have a de Broglie wavelength of about 0.1 nm, about the same as the spacing between atoms in a crystal lattice. If a beam of thermal neutrons is incident on a crystal, the wave nature of the beam will be revealed through a set of interference maxima that occur at angles determined by the Bragg condition:

$$n\lambda = 2d \sin\theta \tag{12.15}$$

where d is the lattice spacing, n the order of the interference maximum, and θ the angle the incident and reflected beams make with the surface of the crystal. This technique, which is used frequently to study the crystalline properties or atomic spacing of materials, is discussed in Section 12.6.

For measurement of the energies of fast neutrons, the most common method is to use the recoil following elastic scattering between the neutron and a light target (H, ^{2}H, ^{3}He, ^{4}He, etc.). This elastic scattering was previously discussed in Section 12.2 in connection with neutron moderation, and we can use the results derived in that section. In the discussion following Equation 12.4, we showed that the scattered neutron has a continuous range of energies from $E' = E$ down to the minimum value given by Equation 12.4. The struck nucleus has a corresponding recoil energy

$$E_R = E - E' \tag{12.16}$$

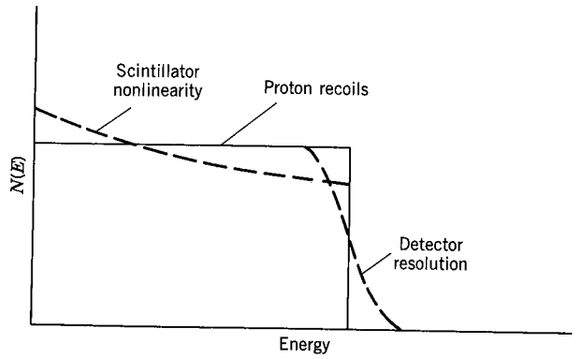

Figure 12.8 An ideal spectrum of proton recoils (from monoenergetic incident neutrons) can be distorted by detector resolution and scintillator nonlinearity.

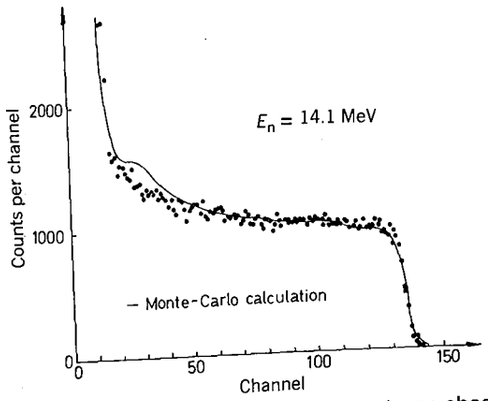

Figure 12.9 Spectrum of monoenergetic 14-MeV neutrons observed in an organic scintillator. From M. Bormann et al., *Nucl. Instrum. Methods* **88**, 245 (1970).

ranging from zero up to a maximum

$$(E_R)_{max} = E - (E')_{min}$$
$$= E\frac{4A}{(A+1)^2} \qquad (12.17)$$

For hydrogen, $(E_R)_{max} = E$, while for ^{3}He, $(E_R)_{max} = 0.75E$. The response of an ideal proton recoil detector to monoenergetic neutrons is shown in Figure 12.8.

The proton recoil signal is normally observed by using a scintillating material that is rich in hydrogen, such as plastic or an organic liquid. The scintillator therefore serves as both the proton target for the neutron and the detector for the recoiling proton. Taking into account the energy resolution of the scintillator and geometrical effects, the observed energy spectrum for monoenergetic neutrons looks like the continuous distribution shown in Figure 12.9. If the incident neutrons have several distinct energy components, the unfolding of the superimposed spectra of recoils may be difficult.

The efficiency of proton-recoil scintillation detectors for MeV neutrons can be of the order of 50%.

12.4 NEUTRON REACTIONS AND CROSS SECTIONS

The formalism for analyzing nuclear reactions has already been discussed in Chapter 11. In this section we give some examples of applications to neutron-induced reactions and show the specific aspects of nuclear structure that can be probed.

Let's first consider the $1/v$ dependence of the low-energy neutron cross section. We can obtain this result using two very different approaches. In Section 11.8, we obtained an estimate for the reaction cross section, Equation 11.50, of

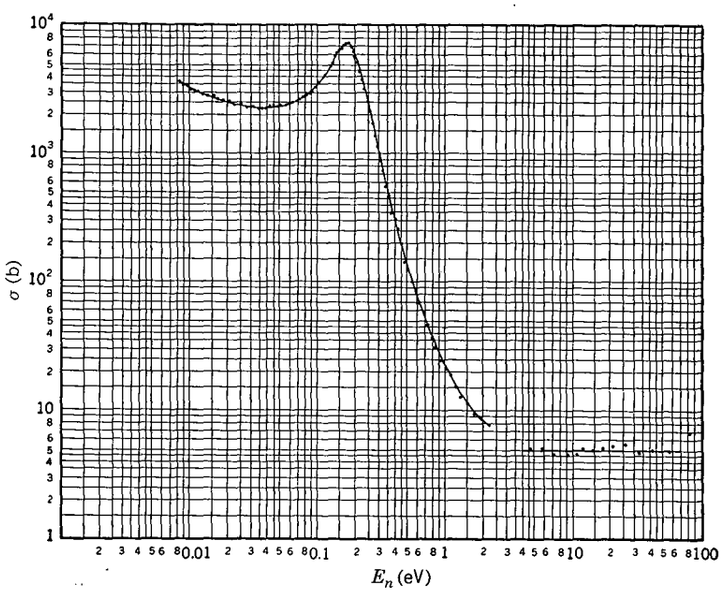

Figure 12.10 Resonances in neutron total cross sections. (*a*) A single isolated resonance superimposed on a $1/v$ background in Cd. (*b*) Several close-lying resonances in In. (*c*) Many sharp peaks in the resonance region in ^{238}U. (*d*) In ^{32}S, the relative heights of the resonance peaks are indications of the spin of the resonances. *Sources*: (*a*), (*b*) H. H. Goldsmith et al., *Rev. Mod. Phys.* **19**, 259 (1947); (*c*) D. J. Hughes and R. B. Schwartz, Brookhaven National Laboratory Report BNL 325 (1958); (*d*) J. M. Blatt and V. F. Weisskopf, *Theoretical Nuclear Physics* (New York: Wiley, 1952).

$\sigma_r = \pi(R + \lambda\!\!\!^{-})^2$ based on a total absorption model. A primary modification to this estimate would include the reflection of the incident neutron wave function at the nuclear surface—how likely is it that the incident particle will penetrate to the region of nuclear potential, where it can be absorbed?

The transmission probability for a rectangular potential barrier was calculated in Section 2.3, and including this factor the cross section is estimated as

$$\sigma = \pi(R + \lambda\!\!\!^{-})^2 \frac{4kK}{(k + K)^2} \tag{12.18}$$

where $K = \sqrt{2m(E + V_0)/\hbar^2}$ for a barrier of depth $-V_0$, and $k = \sqrt{2mE/\hbar^2}$.

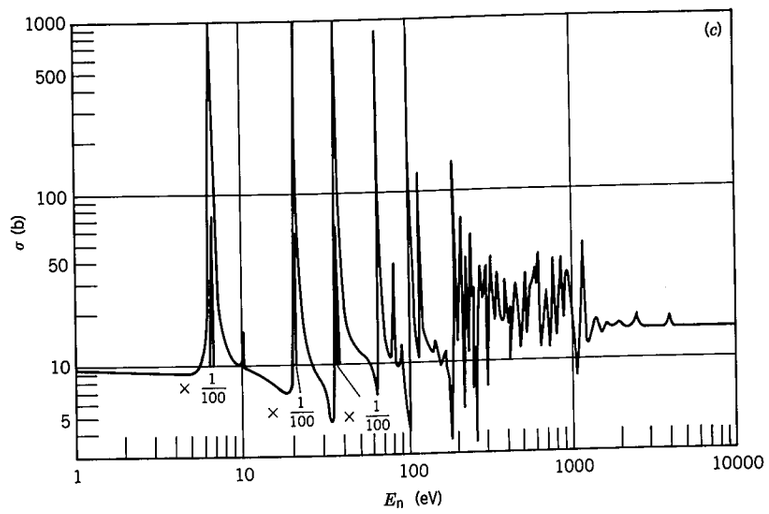

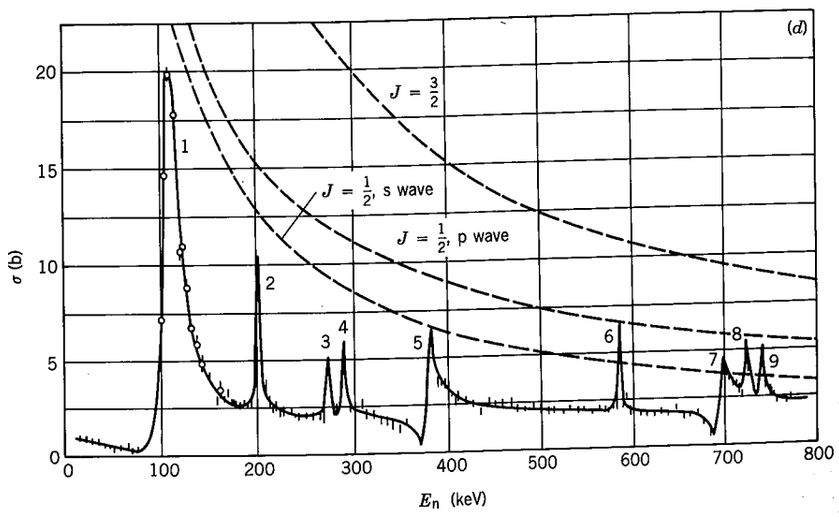

Figure 12.10 Continued.

For low-energy neutrons, $E \ll V_0$ and $k \ll K$; also $\lambda\!\!\!^{-} = k^{-1} \gg R$, so

$$\sigma \cong \frac{4\pi}{kK} \tag{12.19}$$

and since $k = p/\hbar = mv/\hbar$, we have the $1/v$ dependence of the cross section.

A similar result can be obtained from quite another approach, using the single-level resonance formula, Equation 11.70. Following neutron capture, the primary decay mechanism is γ emission, the probability for which is virtually independent of any small variation in the resonance or incident energy. We can therefore take Γ as independent of the neutron energy. The neutron width Γ_n, which refers to the entrance channel, is dependent on the density of final states dn/dE available to the captured neutron, which according to Equation 9.15 is proportional to the velocity of the neutron. (This is somewhat similar to α decay, in which the decay probability includes a factor proportional to v that originates from considering the frequency with which the α particle presents itself to the nuclear barrier in preparation for decay.) Far from the resonance, $E \ll E_R$ and

$$\sigma \cong \frac{\pi}{k^2} \frac{\Gamma_n \Gamma}{E_R^2 + \Gamma^2/4} \propto \frac{1}{v} \tag{12.20}$$

when $\Gamma_n \propto v$.

As indicated by the cross sections plotted in Figure 12.5, the $1/v$ law is followed quite accurately for reactions far from the resonance region.

In the resonance region there is no exact theory for predicting the location of the resonances; the structure may be dominated by a single, isolated resonance (as in Cd, Figure 12.10*a*), or a complex structure (as in In and U, Figures 12.10*b*

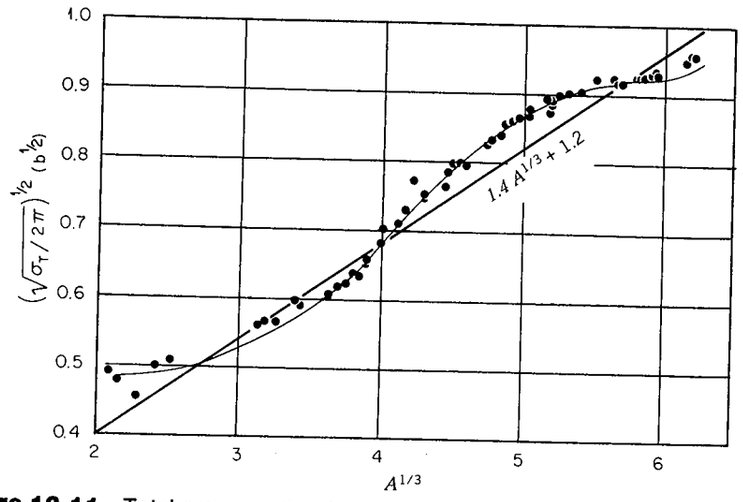

Figure 12.11 Total cross section for 14-MeV neutrons, plotted against $A^{1/3}$. The straight line represents $R + \lambda\!\!\!^{-} = 1.4A^{1/3} + 1.2$ fm, and it fits the data reasonably well. The curve through the data points is an improved calculation using the optical model. From G. R. Satchler, *Introduction to Nuclear Reactions* (Halstead: New York, 1980).

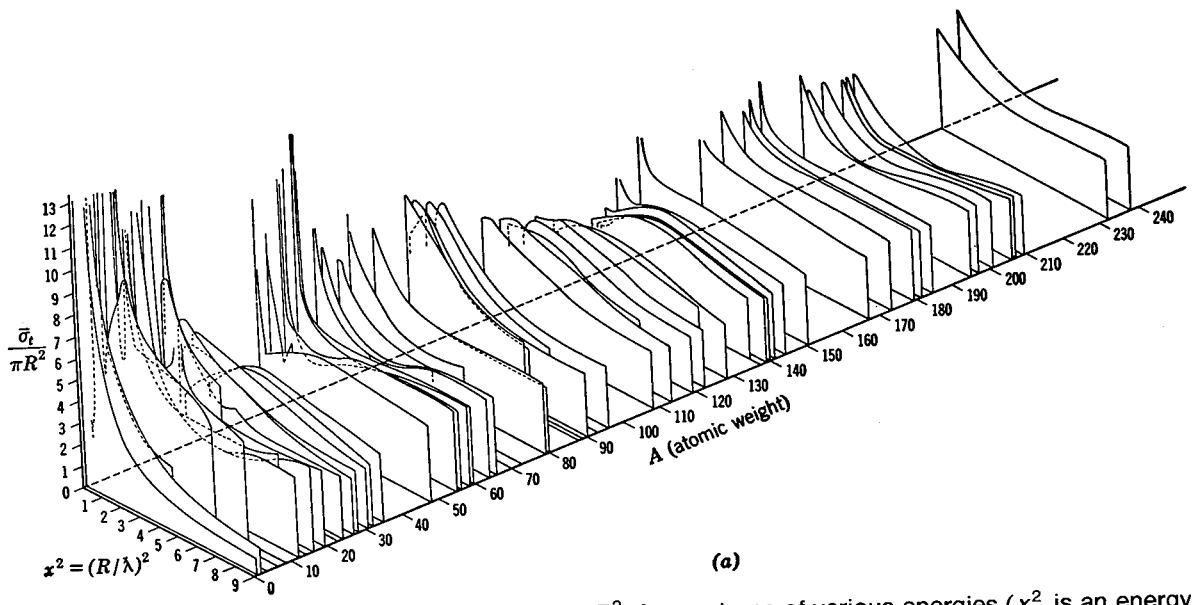

Figure 12.12 The total cross section, in units of πR^2, for neutrons of various energies (x^2 is an energy parameter in dimensionless form). The top curves (*a*) represent experimental results, and the bottom curves (*b*) are the results of calculations using the optical model.

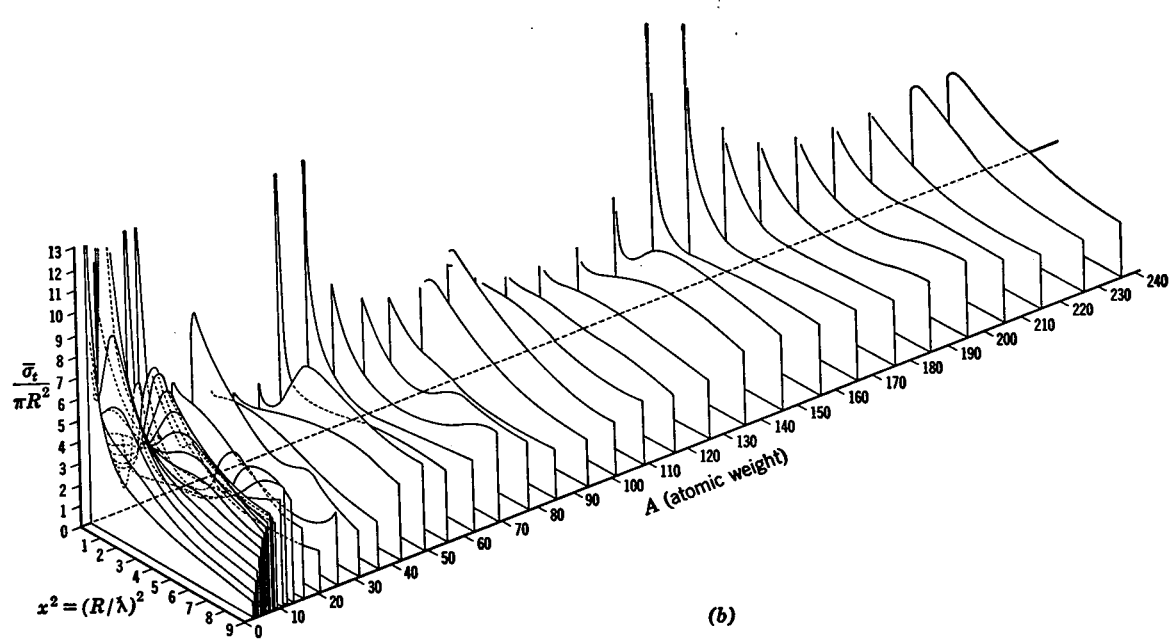

Figure 12.12 Continued.

and c). In some cases, the intensity of a resonance can be used to determine its spin. For instance, in the resonance structure of ^{32}S (which is an even-even, spin zero nucleus), s-wave capture leads to a resonance with total spin $I = \frac{1}{2}$ (from the intrinsic spin of the neutron). P-wave capture can give $I = \frac{1}{2}$ or $\frac{3}{2}$, depending on whether the ℓ and the s of the neutron are antiparallel or parallel. The relationship between the cross section at resonance and ℓ is slightly more complicated than the $(2\ell + 1)$ dependence predicted in Equation 11.47, but the general effect of the increase in cross sections is apparent.

As we move to higher incident energies, the microscopic properties become less important because the observed structure often represents an average over many overlapping resonances. An indication of the applicability of an average property is obtained from the geometrical estimate for the *total* cross section, Equation 11.51. Figure 12.11 shows the quantity $(\sigma_t/2\pi)^{1/2}$ plotted to show $R + \lambda\!\!\!^{-}$, where $R = R_0 A^{1/3}$ and $\lambda\!\!\!^{-} = 1.2$ fm for 14-MeV neutrons. The radius R_0 is taken as 1.4 fm, somewhat larger than the usual estimate of 1.25 fm because it takes into account the skin thickness of the nuclear interaction.

The variations of the total cross section with energy and with A are indicated by Figure 12.12. We can use the optical model (Section 11.9) to calculate the neutron total cross section for these nuclei, with the results also shown in Figure 12.12. The agreement with the observed gross structure is reasonably good.

12.5 NEUTRON CAPTURE

Figure 12.13 shows some of the processes that can occur following neutron capture. Although it is of course possible to re-emit the neutron, for heavy nuclei and very low energy incident neutrons this mode of decay of the compound or resonant state is suppressed, and γ emission is the most probable decay process.

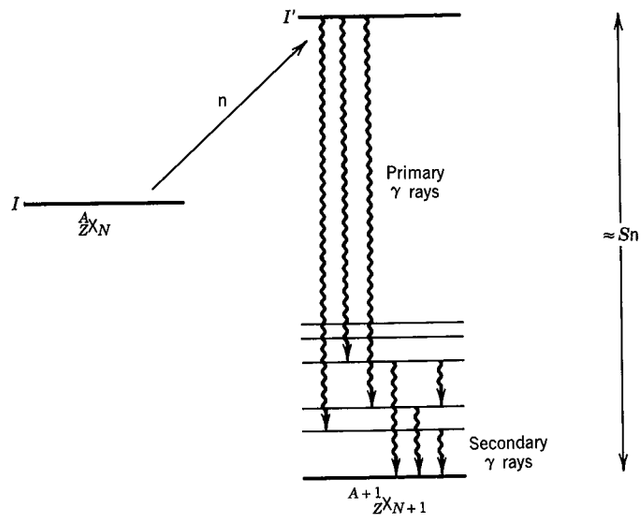

Figure 12.13 Low-energy neutron capture leads to a state I', which emits primary γ rays followed by secondary γ rays.

(Charged-particle emission is inhibited by the Coulomb barrier and unlikely to occur in any but the very lightest nuclei.) The excitation energy E_x of A' is just $S_n + E_n$, the neutron separation energy plus the energy of the incident neutron. For low-energy neutrons, E_x is typically 5–10 MeV.

Neutron capture reactions can be used to determine the energy and spin-parity assignments of the capturing states. Let's assume the original nucleus had spin I and parity π (+ or −). The spin I' of the capturing state is determined by the neutron orbital angular momentum ℓ and spin angular momentum s added to that of the target nucleus:

$$\boldsymbol{I}' = \boldsymbol{I} + \boldsymbol{\ell} + \boldsymbol{s} \tag{12.21}$$

and the parities are related by

$$\pi' = \pi(-1)^{\ell} \tag{12.22}$$

For incident neutrons in the thermal range of energies, only s-wave capture will occur, for which $I' = I \pm \frac{1}{2}$ (excepting $I = 0$, in which case $I' = \frac{1}{2}$ only) and $\pi' = \pi$.

The capture state can usually be treated as a compound-nuclear state, that is, as many unresolved individual levels having $I' = I + \frac{1}{2}$ and $I' = I - \frac{1}{2}$. Occasionally, the capture may be dominated by one or a few resonances, and in certain selected cases it is possible to populate only only the $I' = I + \frac{1}{2}$ or $I' = I - \frac{1}{2}$ resonances by aligning the spins of the target nuclei either parallel or antiparallel to the neutron spins.

In the γ decay of the capture state, all excited states of A' can be populated to some extent, limited only by the selection rules for γ radiation. For dipole radiation, the maximum change in spin is one unit, and thus the primary radiation (that which comes directly from the capture state) reaches states with spins from $I' + 1$ to $I' - 1$. Taking into account the relationship between I' and I, the excited states populated by the primary radiation will have spins ranging from $I - \frac{3}{2}$ to $I + \frac{3}{2}$ (except for $I \leq 1$). For dipole radiation, the emission probability is proportional to E_γ^3, as in Equation 10.12. It is therefore most likely to observe the highest energy transitions, that is, those that populate the lowest excited states. The γ spectrum therefore shows two principal components: the *primary* component, consisting of direct 5–10-MeV radiations from the capture state to lower excited states, usually below 2 MeV, and the *secondary* component, consisting of low-energy radiations between the low-lying excited states.

Electric dipole primary radiation is roughly 100 times more likely than magnetic dipole, and so it is most likely to populate lower excited states whose parity is opposite to that of the capture state. However, magnetic dipole radiation is often present, as is radiation of multipole order higher than dipole; these radiations are usually far less intense than the electric dipole radiation.

One of the useful features in studying neutron capture γ rays is that the primary radiation is almost completely unselective in populating the lower excited states—no strong selection rules based on nuclear structure will forbid primary decays to any particular excited state. Thus if, for instance, the capture state has $I' = 4$, we expect dipole radiation to populate directly *all* spin 3, 4, and 5 states. This is in contrast to α or β decay, in which the emission process is governed by selection rules which may forbid decays to states that, considering

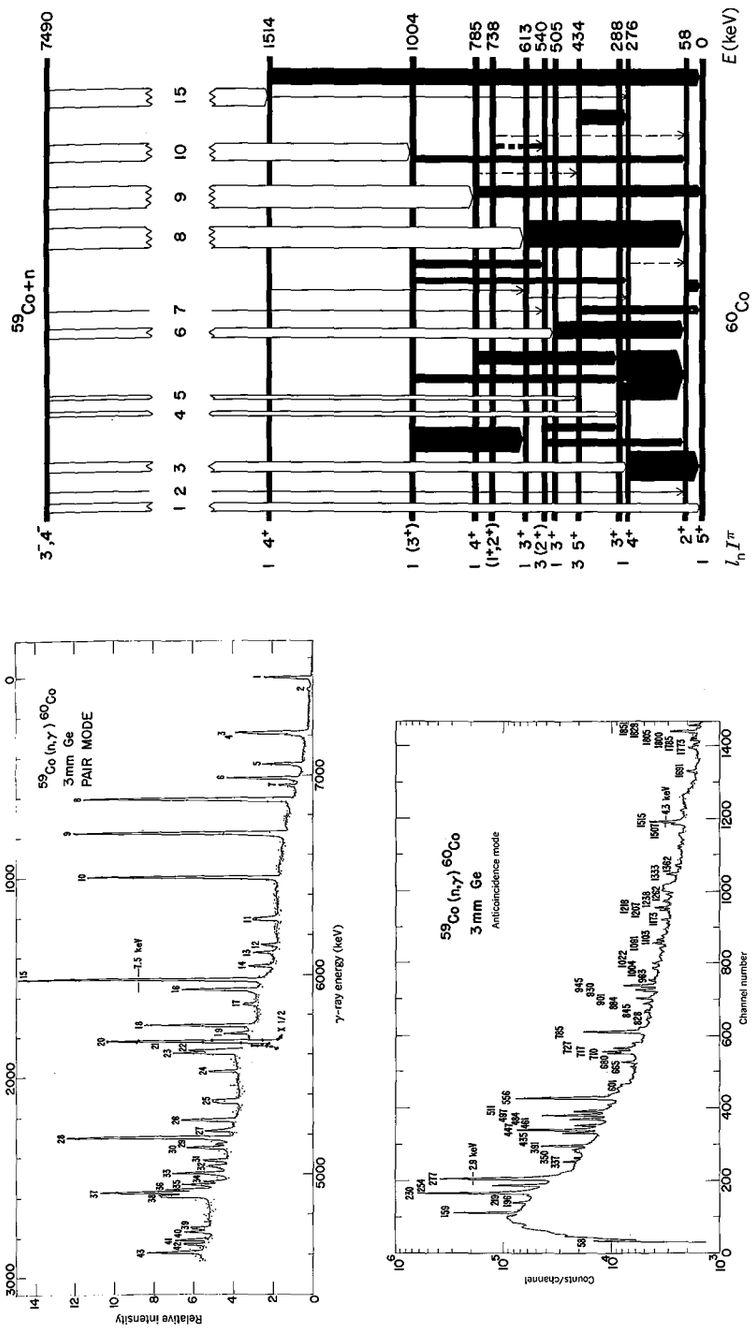

Figure 12.14 Gamma rays following thermal neutron capture by ^{59}Co. (Top left) Primary transitions from the capture state, shown in white on the level scheme at right. (Bottom left) Secondary transitions between the low-lying excited states, shown in black at right. Because ^{59}Co has spin $\frac{7}{2}$ and negative parity, the capture state must be a combination of spin-parity 3^- and 4^-. Electric dipole primary transitions will populate only low-lying 2^+, 3^+, 4^+, and 5^+ states, as shown. No primary transition leading to the 1^+ state at 738 keV is expected, and none is observed. Because the capture state is mostly 4^-, the 2^+ states are only weakly populated (the thickness of the lines at right is proportional to the transition intensity); note transitions number 2 and 7. Data from E. B. Shera and D. W. Hafemeister, *Phys. Rev.* **150**, 894 (1966).

angular momentum couplings only, we might expect to be populated. Neutron capture can therefore serve as a rather *complete* means of spectroscopy of excited states—if we can only unravel what must be a very complicated spectrum of radiations, we should be able to learn a great deal about the number and location of excited states.

Figure 12.14 shows an example of the primary and secondary γ radiations emitted following neutron capture, including the detailed structure of the excited states that can be deduced.

Another application of the (n, γ) reaction occurs when the ground state (or a long-lived isomeric state) of A' is itself radioactive. We therefore accumulate activity of A' (usually without bothering to observe the decay γ's from the capture state). The activity builds up according to Equation 6.24, which can be expressed in the following useful form:

$$\mathscr{A} = 0.602 \frac{m}{A} \sigma \frac{\phi}{3.7 \times 10^{10}} (1 - e^{-\lambda t}) \tag{12.23}$$

where $\mathscr{A}$ is the activity in Curies, m/A is the dimensionless ratio between the mass of the target and its atomic mass, σ is the capture cross section (usually for thermal neutrons) in units of barns, ϕ is the neutron flux in neutrons/cm^2/s, and t is the duration of the neutron bombardment.

This technique has a variety of applications: with a known cross section, measuring $\mathscr{A}$ gives the neutron flux, and thus we have a measure of neutron intensity. If ϕ is known, on the other hand, we can determine unknown cross sections. The most common application, however, is to use cases with known ϕ and σ to do qualitative analysis to determine m. After exposing an unknown sample to neutrons, we can observe many different radiations from the radioactive decays of those isotopes that can be produced by neutron capture. Careful measurement of the γ-ray spectrum permits the determination of which isotopes are present and in what quantities, and we can thus deduce the original quantities present in the irradiated sample. This technique is called *neutron activation analysis* and it has important applications in a variety of areas, including environmental pollution research, archeology, and forensic science. We discuss this application of nuclear techniques in Chapter 20.

12.6 INTERFERENCE AND DIFFRACTION WITH NEUTRONS

Beams of neutrons provide an excellent way to observe effects depending on the wave behavior of material particles. In Chapter 11 we saw examples of the diffraction of nucleons in scattering from nuclei, in cases in which the wavelength of the incident particle was comparable to the nuclear size. By moving to other ranges of wavelengths, however, we can observe effects such as single and double slit or thin film interference, which are more frequently demonstrated only with optical radiations.

In Figure 12.15 are shown results from single-slit and double-slit interference experiments. The interference effects are very apparent and remind us of the analogous results using light waves.

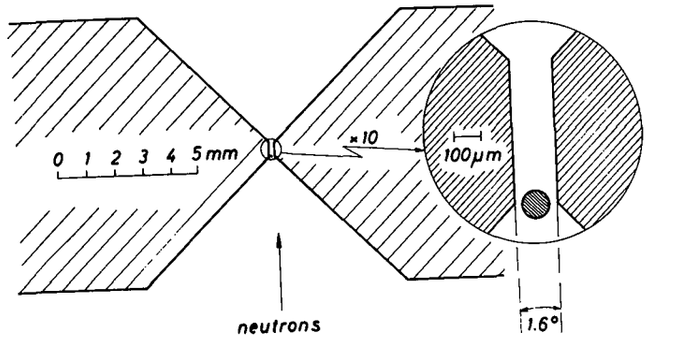

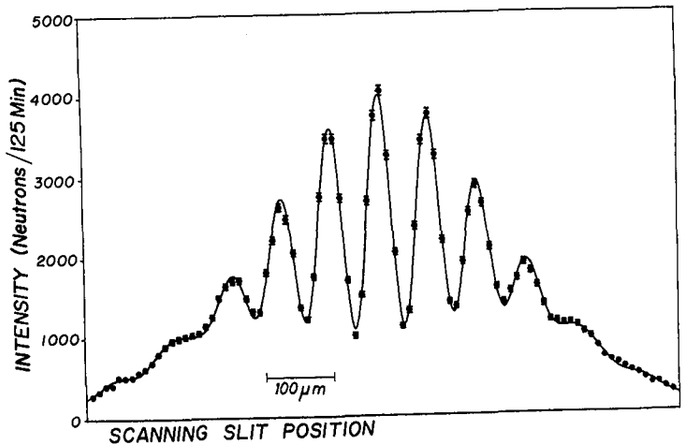

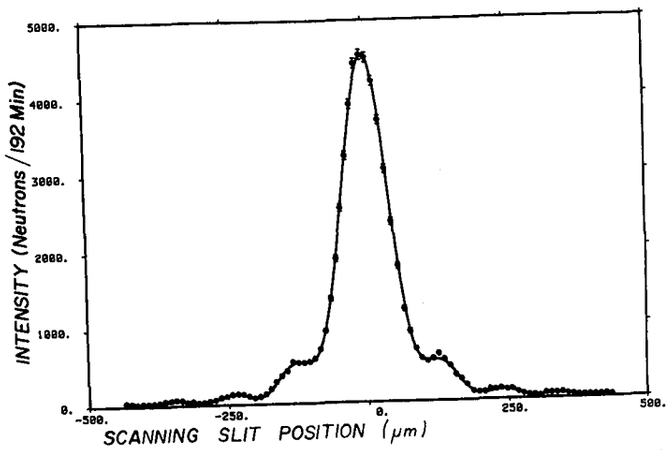

Figure 12.15 (Top) Double-slit apparatus for neutrons. A highly absorbing boron wire is mounted in the gap between two pieces of neutron-absorbing glass to form a double slit. (Middle) Double-slit interference pattern. The dots are the experimental points and the curve is calculated from the Schrödinger equation for a neutron wavelength of 1.845 nm. (Bottom) A single-slit interference pattern. All figures from A. Zeilinger, R. Gaehler, C. G. Shull, and W. Treimer, in *Neutron Scattering—1981*, edited by J. Faber (New York: American Institute of Physics, 1982), p. 93.

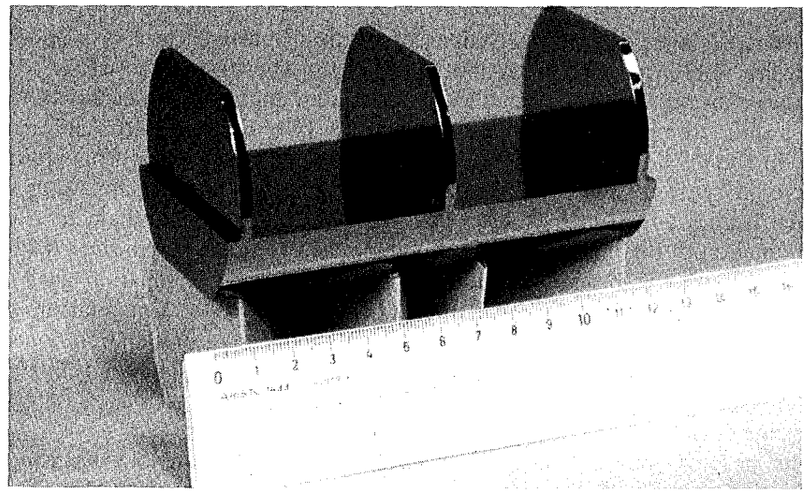

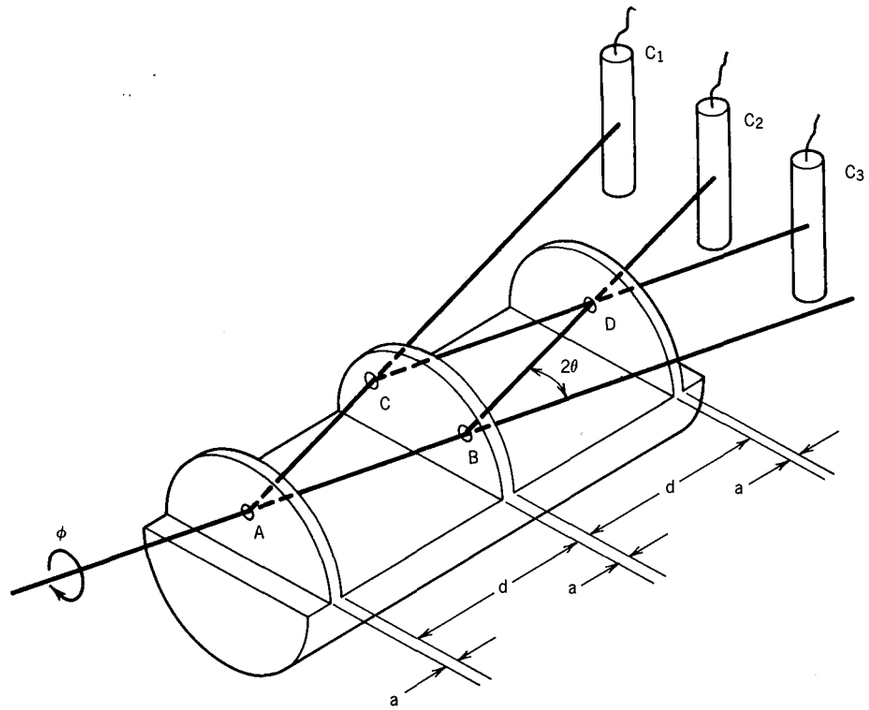

Figure 12.16 (Top) Photograph of neutron interferometer, carved from a single block of silicon 5 cm in diameter and 9 cm long. The three slabs are attached to the base as they were in the original crystal, and therefore the atoms in the slabs are spatially coherent. Photograph courtesy of Professor Samuel A. Werner. (Bottom) Schematic diagram of interferometer. Counter C_1 counts the non-interfering beam, while C_2 and C_3 count the two interfering beams which re-combine at D. From S. A. Werner, J.-L. Staudenmann, R. Colella, and A. W. Overhauser, in *Neutron Interferometry*, edited by U. Bonse and H. Rauch (Oxford: Clarendon Press, 1979), p. 209.

The most ingenious demonstrations of neutron interference have been done with the interferometer shown in Figure 12.16. The device consists of three identical "beam splitters," each of which passes an undeviated transmitted beam and a diffracted beam deflected by an angle 2θ. (We discuss neutron diffraction later in this section.) To obtain identical diffractions at the three beam splitters and to guarantee precise alignment of the three planes, the entire apparatus was carved from a large single crystal of silicon, of length 9 cm and diameter 5 cm. The function of the third slab is to recombine the two interfering beams BD and CD into outgoing beams that contain the interference information as a net intensity variation. (The variations in the two beams are complementary to one another and contain the same information.) Without the recombination done by the third crystal, the interference would occur only at the single point D where the interfering beams cross. Figure 12.17 shows the interference effects observed with this device.

The neutron interferometer has been used in two remarkable experiments which demonstrate aspects of quantum behavior that have not been accessible to testing by any other means. In the first of these, the interferometer was rotated about the horizontal axis AB in Figure 12.16. At a certain value of the rotation angle, one of the beams, ABD for instance, will lie at a greater height than the other (ACD) and will therefore experience a different gravitational potential, mgy. The differing gravitational potential between the two beams causes a relative phase shift that changes the way they interfere when they are recombined. As the angle ϕ (which measures the rotation about the axis) is varied, the intensity in the recombined beam will vary accordingly. Figure 12.18 shows the resulting variation in intenity as ϕ is varied. This experiment, done 50 years after de Broglie's work and after the introduction of the Schrödinger equation, is the first to demonstrate that the Schrödinger equation and the laws of quantum mechanics apply to gravitational fields. The experimental result shows great sensitivity to physical parameters—it was possible to deduce the sag in the crystal caused by bending under its own weight (about 2 nm) and also to observe the Coriolis effect on the two neutron paths due to the rotation of the Earth.

Another unusual and fundamental interferometry experiment with neutrons is done by causing one of the neutron paths (AB, for example) to pass through a magnetic field. In the region of the magnetic field, the magnetic moment of the neutron will precess about the field direction, and this precession causes a change in the phase of the neutron wave function, which is again observed as a variation in the intensity of the recombined beam.

Quantum mechanics predicts an unusual (and previously untested) result for spin-$\frac{1}{2}$ particles—the phase of the wave function upon rotation by an angle α is $e^{is\alpha}$, where s is the spin in units of $\hbar$. When α is 2π (360°), the phase is $e^{i\pi}$ or -1. Thus a complete 360° rotation of the system causes a change in phase of the wave function! This is certainly a nonclassical effect, for in classical physics a 360° rotation leaves all equations unchanged. However, the change in phase of the interfering beams will cause the interference to go from, for instance, a maximum (corresponding to $|\psi|^2 = |\psi_{ACD} + \psi_{ABD}|^2$) to a minimum ($|\psi|^2 = |\psi_{ACD} - \psi_{ABD}|^2$). The neutron interference experiments not only observed the effects of the spin precession of the neutrons, they demonstrated for the first time that a 720° rotation, not a 360° rotation, is required to bring the system back to

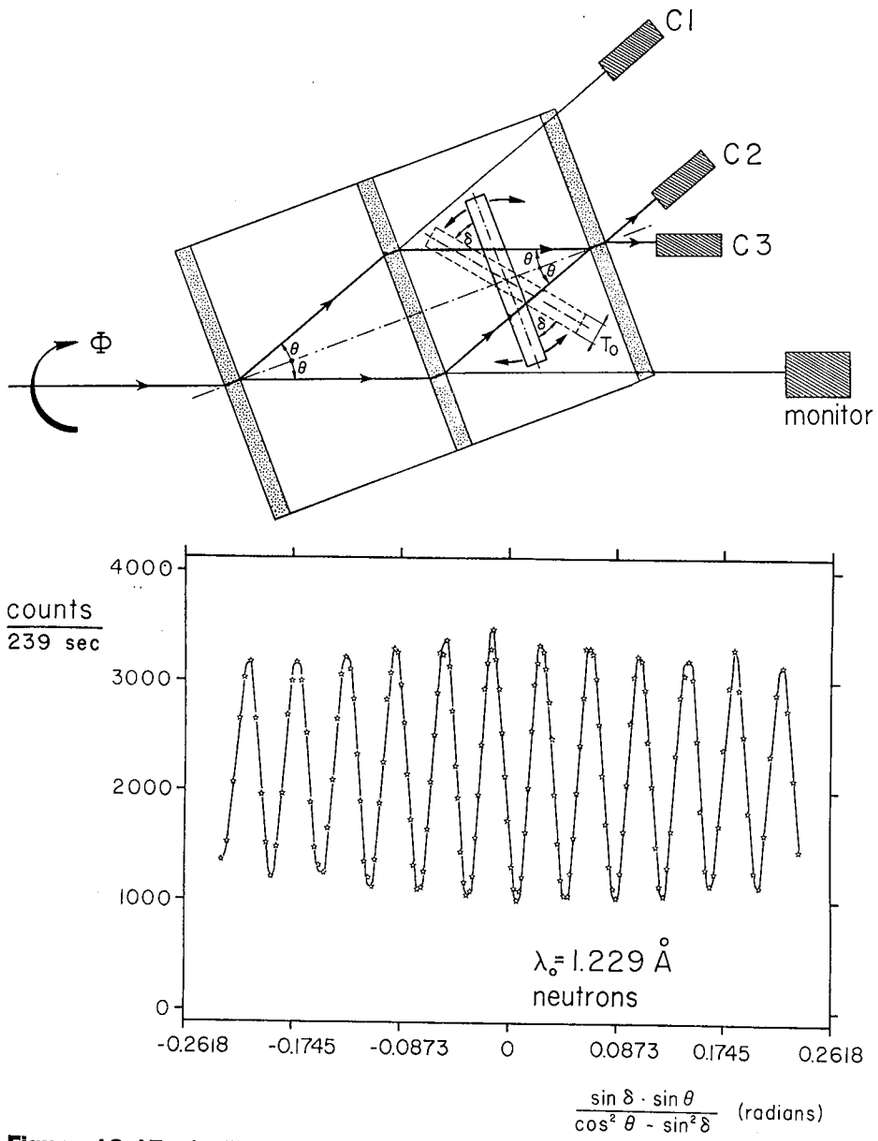

Figure 12.17 A silicon slab placed between the second and third diffracting planes is free to rotate (angle δ in the figure at top). As it does, the two neutron beams must pass through different thicknesses of silicon, which causes a phase shift and a change in intensity when they are recombined. The lower part of the figure shows the observed intensity variation, measured in counter C_3, as δ is varied. From S. Werner, J.-L. Staudenmann, R. Colella, and A. W. Overhauser, in *Neutron Interferometry*, edited by U. Bonse and H. Rauch (Oxford: Clarendon, 1979), p. 209.

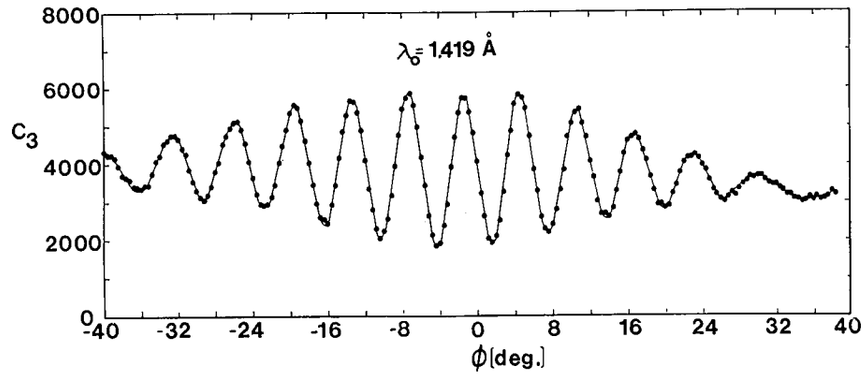

Figure 12.18 Neutron interference in a gravitational field. As the interferometer rotates by the angle ϕ about a horizontal axis, as in Figure 12.17, the two interfering beams change gravitational potentials, which causes a phase difference and a corresponding intensity variation in the recombined beams, as shown. Notice that a rotation of 3–4° changes the counting rate in detector C_3 by a factor of 3. From S. Werner, J.-L. Staudenmann, R. Colella, and A. W. Overhauser, in *Neutron Interferometry*, edited by U. Bonse and H. Rauch (Oxford: Clarendon, 1979), p. 209.

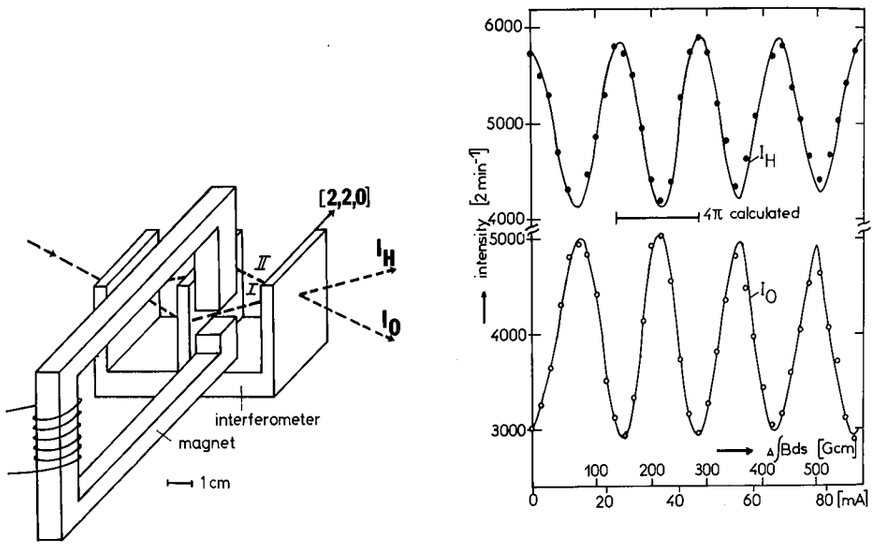

Figure 12.19 Neutron interferometer used to demonstrate rotation of neutron spins in a magnetic field. Unpolarized neutrons of $\lambda = 1.8$ nm are incident on the interferometer; one of the interfering beams passes through the magnetic field, the strength of which may be varied. The neutron spins in branch I precess relative to those in branch II. The data show that a phase change of 4π is necessary to obtain constructive interference. From H. Rauch et al., *Phys. Lett. A* **54**, 425 (1975).

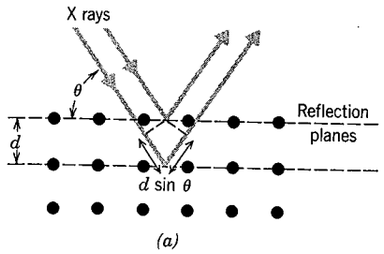

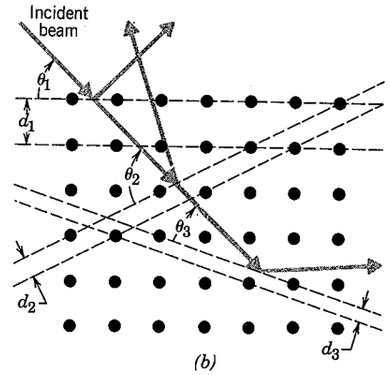

Figure 12.20 (*a*) An incident beam can be reflected from two adjacent parallel rows of atoms in a lattice. If the path difference, $2d \sin\theta$, is an integral number of wavelengths, there will be constructive interference. (*b*) There are many possible ways to choose the set of parallel reflecting lattice planes. Corresponding to each will be a particular value of θ and of d.

its original configuration. Figure 12.19 shows the variation in the interfering intensity as the magnetic field is varied.

Probably the most frequent application of neutron interference is in the diffraction of neutrons by crystals. The diffraction can be used to provide a source or a detector of monoenergetic neutrons, or it can be used to study crystal structures of materials. Figure 12.20 illustrates the basic application of the Bragg law, Equation 12.15, to the diffraction by a single crystal. For neutrons whose wavelengths are about the same order as the crystalline atomic spacing d, interference results in an apparent "reflection" from planes drawn through atoms of the lattice. Typical atomic spacings in solids are of order 0.1 nm, and a de Broglie wavelength of 0.1 nm corresponds to thermal neutron energies.

The choice of a particular set of reflection planes is arbitrary; Figure 12.20 also shows several other choices, corresponding to different angles θ and different spacings d. In three dimensions, we can specify the choice of planes with a set of indices that give essentially the number of fundamental lattice spacings along the three coordinate axes. Figure 12.21 shows some examples of different lattice planes in three dimensions.

The intensity at any particular reflection may be a complicated function of crystal properties and neutron scattering amplitudes (which may involve coherent sums over different isotopes that may be present in the crystal). Figure 12.22 is an example of a scattering spectrum taken for neutrons of a particular wavelength. The scattering sample in this case was a powder consisting of many microcrystals, so that all possible orientations are simultaneously observed.

An alternative approach would be to begin with a beam of neutrons containing a mixture of energies, such as might be obtained from a reactor. If the beam falls on a scattering crystal, at a certain angle (as in Figure 12.23) we will observe monoenergetic neutrons that satisfy the Bragg condition (assuming that the same angle does not happen to satisfy the Bragg condition for a different wavelength and set of crystal planes). If we change the angle θ slightly, the same Bragg condition will be satisfied for a slightly different wavelength or energy. We thus

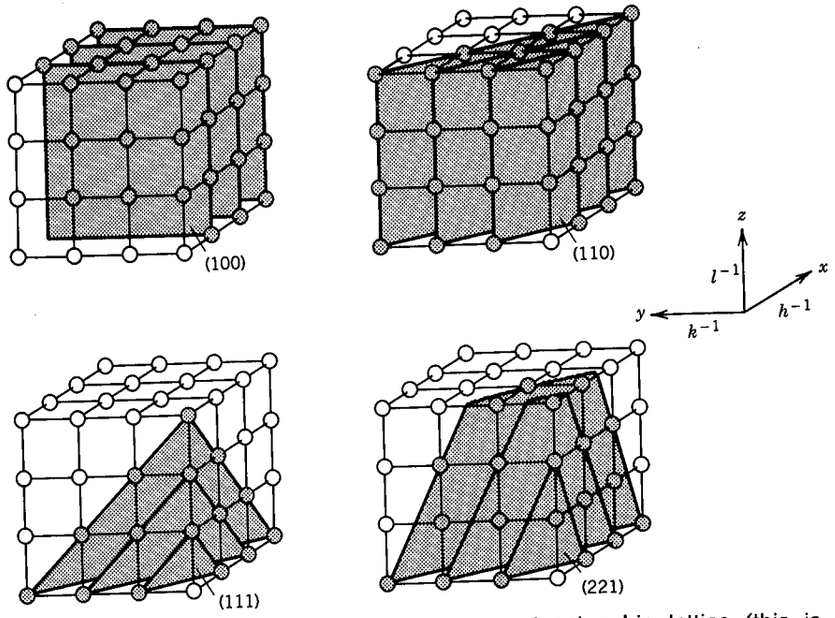

Figure 12.21 Planes of atoms in three-dimensional cubic lattice (this is a three-dimensional analog of Figure 12.20*b*). The indices (*hkl*) give integers in the ratio of the *inverse* of the coordinates of the plane with respect to the three directional axes *x, y, z*. Thus $x = 1$, $y = \infty$, $z = \infty$ (upper left) reduces to (100); $x = 1$, $y = 1$, $z = 2$ (lower right) becomes $(11\frac{1}{2})$ and then (221) by changing to integers in the same ratio.

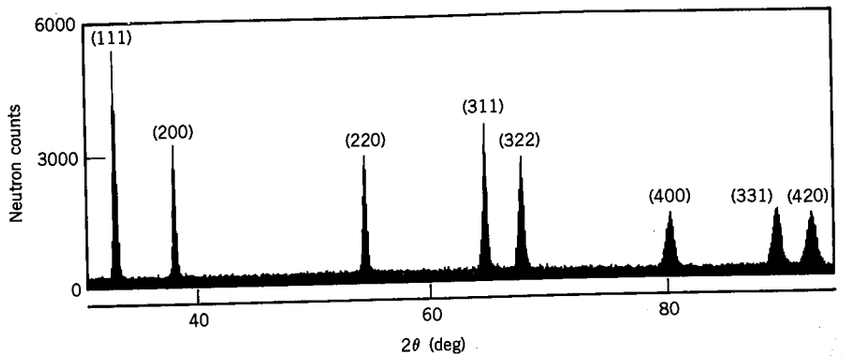

Figure 12.22 Diffraction pattern of nickel powder using incident neutrons of wavelength 0.114 nm. The scattering angle 2θ is plotted, and the peaks are labeled with the indices of the lattice planes, as in Figure 12.21. From G. E. Bacon, *Neutron Diffraction* (Oxford: Clarendon, 1975).

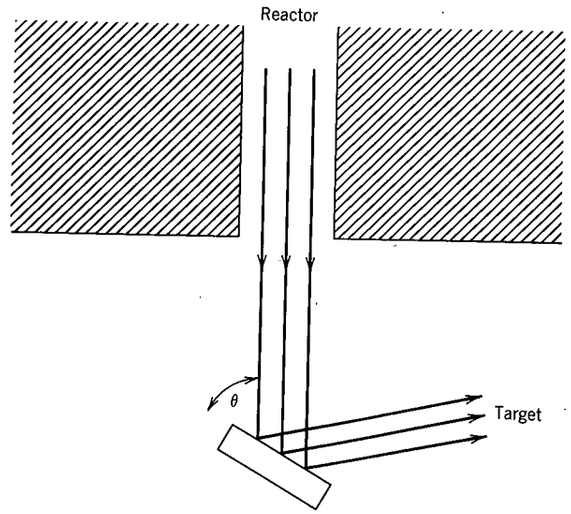

Figure 12.23 Monochromator for producing a beam of monoenergetic neutrons. A collimated beam of reactor neutrons with a broad spectrum of wavelengths is Bragg reflected from a single crystal. For a particular value of θ, there will be an interference maximum for a certain wavelength, and thus by varying θ we can choose the wavelength. As in Figure 12.20*b*, there may be other Bragg reflected peaks at other angles, which are not shown.

have a *neutron monochromator*, a source of neutrons of any particular energy, with a spread in energy determined by the angular spread of the beam.

Powder diffraction patterns such as shown in Figure 12.22 can be used to deduce the type of crystal structure, as in the cubic lattice characteristic of nickel. Similar studies are possible for more complex systems, including the relatively disordered structures of liquids and glasses, and the exceedingly complicated structures of biological molecules.

The primary mechanism for neutron scattering is the nuclear scattering that we have discussed previously in this chapter and in Chapter 11. An alternative mechanism is *magnetic* scattering, in which the neutron magnetic moment scatters from the electronic magnetic moment. If it is possible to separate nuclear from magnetic scattering (as, for instance, by using polarized neutrons), it is possible to deduce magnetic structures, which can be more complicated and more interesting than the physical arrangement of atoms in the lattice. Figure 12.24 shows the neutron diffraction pattern of MnO above and below the Néel temperature, which is for antiferromagnets what the Curie temperature is for ferromagnets. Below the Néel temperature, MnO is antiferromagnetic, in which there are alternating layers with opposite spin orientations. (In a ferromagnetic structure, all spins would be parallel.) Figure 12.25 shows a representation of the structure. The basic distance needed for the structure to repeat itself (called the *unit cell* dimension) is twice what it would be if we were above the Néel temperature where the magnetic structure repeats in nonalternating fashion. There is a factor of 2 difference in the basic distance d that appears in the Bragg

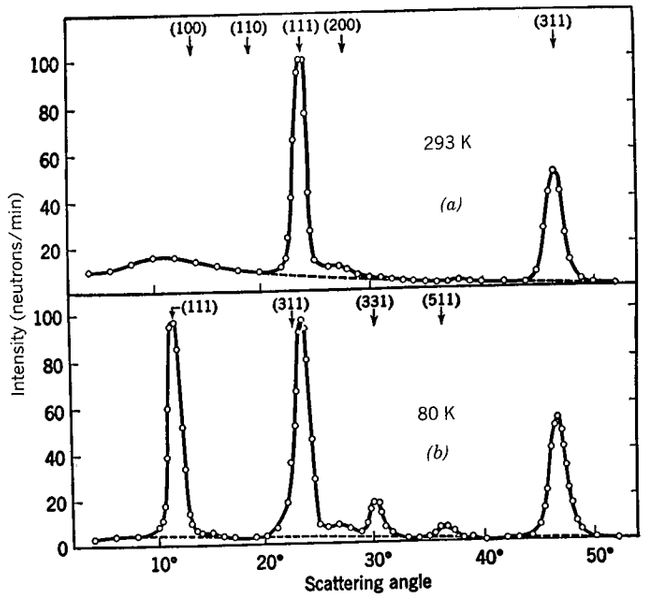

Figure 12.24 The neutron diffraction pattern of MnO (*a*) above and (*b*) below the antiferromagnetic transition temperature. Notice the factor of 2 difference in the location of the 111 peak. From C. G. Shull and J. S. Smart, *Phys. Rev.* **76**, 1256 (1949).

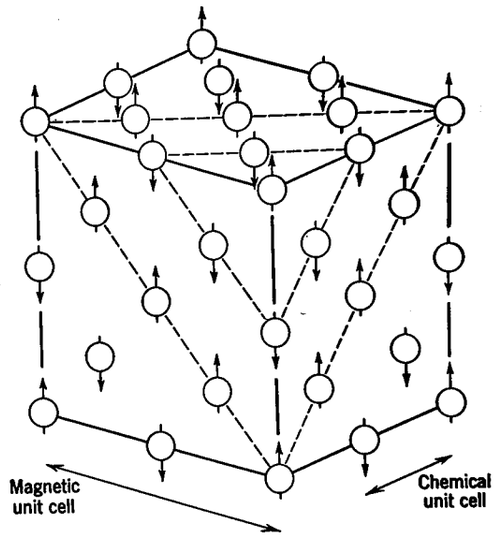

Figure 12.25 The crystal structure of MnO. In the antiferromagnetic structure, the lattice repeats over a distance of $2a$ (where a is the spacing of the Mn atoms) while at high temperature the spins are all aligned and the lattice repeats over a distance of a.

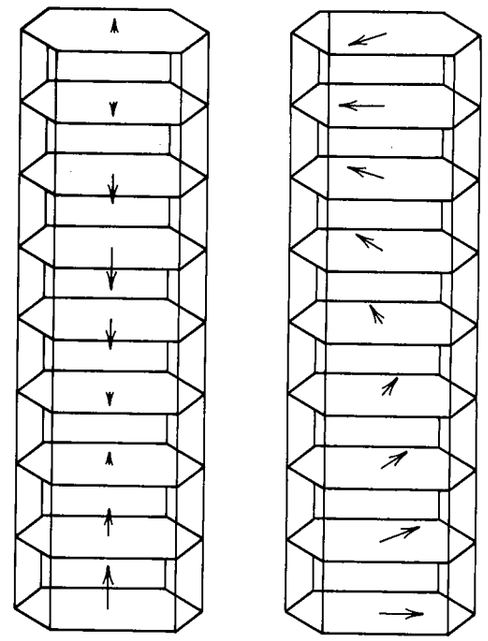

Figure 12.26 Two examples of rare-earth magnetic structures studied by neutron diffraction. The basic crystal structure is that of stacked planes of hexagonal arrays of atoms. The arrows show the effective magnetic dipole moments. The structure at left is characteristic of erbium metal in the temperature range 52–85 K, and that at right describes terbium in the range of 220–230 K. Below 220 K, the terbium moment does not rotate from one plane to the next, but points in a fixed direction. Below 20 K, erbium shows a moment that has a rotating component in the hexagonal plane and a perpendicular component of fixed magnitude.

equation, and the result is that the peaks for magnetic scattering appear at values of θ such that $\sin\theta$ is half what it would be for nuclear scattering.

The rare-earth metals have rather similar crystal structures of the hexagonal type, but very different magnetic properties that also change with temperature as in the case of MnO. In some cases the electronic magnetic moment is perpendicular to the hexagonal plane, but may be modulated in unusual ways from one layer to the next, as for example several layers pointing up and then several down, or else sinusoidally. In other structures, the electronic moment lies in the hexagonal plane, but it rotates through a certain angle from one layer to the next. These magnetic structures, illustrated in Figure 12.26, can be studied only through neutron diffraction.

REFERENCES FOR ADDITIONAL READING

A nontechnical introduction to neutron physics is D. J. Hughes, *The Neutron Story* (New York: Doubleday, 1959). Modern research with extremely low-energy neutrons is described in "Ultracold Neutrons" by R. Golub, W. Mampe, J. M. Pendlebury, and P. Ageron in the June 1979 issue of *Scientific American*.

For general surveys of neutron physics, see L. F. Curtiss, *Introduction to Neutron Physics* (Princeton, NJ: Van Nostrand, 1959); D. J. Hughes, *Pile Neutron Research* (Cambridge: Addison-Wesley, 1953); D. J. Hughes, *Neutron Optics* (New York: Interscience, 1954).

For more advanced and detailed references, see I. I. Gurevich and L. V. Tarasov, *Low-Energy Neutron Physics* (Amsterdam: North-Holland, 1968); J. E. Lynn, *The Theory of Neutron Resonance Reactions* (Oxford: Clarendon, 1968); *Fast Neutron Physics*, edited by J. B. Marion and J. L. Fowler (New York: Interscience, 1960); C. G. Windsor, *Pulsed Neutron Scattering* (New York: Halsted, 1981).

A comprehensive survey of neutron diffraction is G. E. Bacon, *Neutron Diffraction*, 3rd ed. (Oxford: Clarendon, 1975).

Reports on recent work with neutrons can be found in *Neutron Sources for Basic Physics and Applications*, edited by S. Cierjacks (Oxford: Pergamon, 1983); *Neutron Interferometry*, edited by U. Bonse and H. Rauch (Oxford: Clarendon, 1979); *Neutron Scattering—1981*, edited by John Faber, Jr. (New York: American Institute of Physics, 1982).

PROBLEMS

1. In the reaction $\alpha + {}^{9}\mathrm{Be} \rightarrow {}^{12}\mathrm{C} + \mathrm{n}$, find the maximum and minimum neutron energies when the incident α energy is (a) 7.0 MeV; (b) 1.0 MeV.
2. If the neutrons in Problem 1 are emitted uniformly in space, sketch their energy spectrum, that is, the relative number emitted at each energy from the minimum to the maximum.
3. A 5.00-MeV proton beam is available to produce neutrons from the reaction ${}^{7}\mathrm{Li(p, n)}{}^{7}\mathrm{Be}$. A neutron beam of 1.75 MeV is needed for a particular experiment. (a) In what direction relative to the incident beam should we look to find 1.75-MeV neutrons? (b) If we extract the neutrons through a 1-cm aperture located 10 cm from the reaction target, what will be the energy spread of the neutron beam?
4. Neutrons were first observed through the "knock-on" protons produced in direct head-on scattering. If protons are observed at an energy of 5.3 MeV, compute the incident energy if the incident particle is (a) a photon, or (b) a neutron.
5. A neutron of kinetic energy E scatters elastically from a target atom at rest. Find the maximum energy lost by the neutron if the target is (a) ${}^{2}\mathrm{H}$; (b) ${}^{12}\mathrm{C}$; (c) ${}^{238}\mathrm{U}$.
6. For neutron moderation by protons, make a sketch showing the average energy of a beam of initial 2.0-MeV neutrons as a function of time, assuming the mean time between collisions is t. How long does it take for the neutrons to lose 50% of their energy? How long for 90%?
7. A point source of fast neutrons (a radium-beryllium source, for example) is placed at the center of a tank of water. Make a sketch showing the density of thermal neutrons as a function of the distance from the source. Your sketch should indicate general features only; don't try to be too specific. The mean free path of neutrons in water is a few centimeters for fast neutrons to a few tenths of a centimeter for slow neutrons.

8. Derive Equation 12.7.
9. Find the number of collisions necessary to reduce the energy of a 1 MeV neutron to 1 eV in scattering by (a) hydrogen; (b) carbon; (c) beryllium; (d) iron.
10. In scattering between incident neutrons and target protons at rest, show that the angle between the two scattered particles is always 90°.
11. The intensity of a source of thermal neutrons is to be measured by counting the induced radioactivity in a thin foil of indium metal exposed to the neutrons. The foil is 3.0×3.0 mm in area and 1.0 μm in thickness. The activation of ${}^{115}\mathrm{In}$ to ${}^{116}\mathrm{In}$ ($t_{1/2} = 54$ min) takes place with a cross section of 160 b for thermal neutrons. The foil is irradiated for 1 min, but after the conclusion of the irradiation, the counting of the decays from the foil cannot be started for 30 min. The efficiency of the detecting system is only 2.4×10^{-4}, and in 1 h of counting 4.85×10^{4} counts are accumulated. What is the thermal neutron flux?
12. In low-energy neutron capture by ${}^{55}\mathrm{Mn}$, the following primary γ transitions are seen (energies in MeV): 7.2703, 7.2438, 7.1597, 7.0578, 6.9287. (a) Deduce the corresponding energies of the ${}^{56}\mathrm{Mn}$ excited states. (b) ${}^{55}\mathrm{Mn}$ has $I^{\pi} = \frac{5}{2}^{-}$. What are the possible I^{π} assignments of the ${}^{56}\mathrm{Mn}$ excited states populated through primary transitions?
13. (a) ${}^{143}\mathrm{Nd}$ has a $\frac{7}{2}^{-}$ ground state. Following thermal neutron capture, would you expect to see a strong primary transition from the capture state to the ${}^{144}\mathrm{Nd}$ ground state? (b) Would you expect the same in the case of capture by ${}^{119}\mathrm{Sn}$ ($\frac{1}{2}^{+}$)?
14. A beam of neutrons of energy 50 keV is incident on a slab of graphite of thickness 2.5 cm. The transmitted beam has intensity of 26% of the original beam. What value does this indicate for the scattering phase shift? (It is a good approximation to neglect all but the s-wave phase shift. Why?)
15. A beam of neutrons of wavelength λ is incident in the x direction on a crystal represented by the cubic lattice of Figure 12.21. The spacing between neighboring atoms along the coordinate axes is a. (a) Find the spacing d between the lattice planes for the 4 cases in terms of a. (b) Find the direction in space of the scattered neutrons in each case for the first-order interference.